Applied Energy 134 (2014) 374–381

Contents lists available at ScienceDirect

Applied Energy

journal homepage: www.elsevier.com/locate/apenergy

Analytic thermoelectric couple optimization introducing Device Design Factor and Fin Factor

J. Mackey [a,*], A. Sehirlioglu [b], F. Dynys [c]

[a] Department of Mechanical Engineering, University of Akron, Akron, OH 44325, USA
[b] Department of Materials Science and Engineering, Case Western Reserve University, Cleveland, OH 44106, USA
[c] NASA Glenn Research Center, Cleveland, OH 44135, USA

HIGHLIGHTS

- We introduce a Device Design Factor to account for thermal losses of a thermoelectric couple.
- We introduce a Fin Factor to account for lateral heat transfer in a thermoelectric couple.
- Conversion efficiency is analytically derived in terms of new design parameters.

ARTICLE INFO

Article history:
Received 24 April 2014
Received in revised form 5 August 2014
Accepted 7 August 2014
Available online 29 August 2014

Keywords:
Thermoelectric modeling
Seebeck coefficient
Peltier effect

ABSTRACT

An analytic solution of a thermocouple has been developed in order to gain a deeper understanding of the physics of a real device. The model is established for both rectangular and cylindrical couples and is made to account for thermal resistance of the hot and cold shoes and lateral heat transfer. A set of dimensionless parameters have been developed to determine couple behavior and serve as simplifying justifications. New dimensionless parameters, Device Design Factor and Fin Factor, are introduced to account for the thermal resistance and lateral heat transfer, respectively. Design guidelines on couple length and cross-sectional area have been established to account for conditions encountered by a realistic couple. As a result of thermal resistances a lower limit on the length of the couple can be established. In the case of a lateral heat transfer couple the efficiency is found to depend upon cross-sectional area of the leg in such a fashion as to suggest the need to design large area couples. The classic thermoelectric solution neglects the effect of thermal resistance and lateral heat transfer, leading to an over estimated conversion efficiency. The work presented provides a path to incorporate these neglected factors and offers a simplified estimation for couple performance based on analytic solutions of governing equations.

1. Methodology

The foundation of the thermoelectric device is the fundamental thermoelectric couple, composed of two conducting legs classically configured electrically in series and thermally in parallel. The coupled transport of thermal and electrical energy through the legs serves to operate as a heat pump or heat engine depending on the driving mechanism. Therefore it is of critical interest to have a clear understanding of the physics of a thermoelectric couple in order to design both materials and devices capable of providing the desired thermoelectric output in an efficient and optimized manner.

The governing equations of a couple can be derived from applying the generalized thermoelectric form of Ohm's and Fourier's Laws to a control volume, obtainable from the conjugate flux force relations of Onsager [1,2]. A similar approach can be found in the classic conduction equation in many heat transfer texts, such as Arpaci [3], Ozisik [4], and Carslaw and Jaeger [5]. The couples were investigated as steady state one dimensional domains, neglecting temperature and electrical gradients in directions other than the primary leg length, and with constant material properties. Steady state is justified by common application of devices, and for the purpose of obtaining concise solutions. Investigation into transient behavior has been performed by Meng et al. [6], Alata et al. [7], and Montecucco et al. [8] among others. The one dimensional assumption can be justified by investigating Biot numbers for the primary leg direction versus the lateral direction of typical thermoelectric legs. The constant material properties simplification was

* Corresponding author. Tel.: +1 (216)433 3901.
E-mail address: jam151@zips.uakron.edu (J. Mackey).

http://dx.doi.org/10.1016/j.apenergy.2014.08.034
0306-2619/

used to form a linear model so that meaningful solutions could be developed. The effect of variable material properties is out of the scope of this work. Some of the effects of variable material properties may be accounted for by incorporating the standard integral-averaged approach for the calculation of the typical thermoelectric properties, see Sandoz-Rosado and Stevens [9].

The resulting system model consists of four coupled ordinary differential equations and a fifth coupled algebraic Eqs. (1)–(3). Eq. (1) gives the thermal governing equations for two legs, **a** and **b**, while Eq. (2) gives the electrical governing equations for the same legs. The fifth equation (Eq. (3)) represents Ohm's Law.

$$-\frac{d^2\widehat{T}_{a,b}}{d\hat{x}^2}+\beta_{a,b}\widehat{I}_{a,b}\frac{d\widehat{T}_{a,b}}{d\hat{x}}-\gamma_{a,b}\widehat{I}_{a,b}^2=0, \tag{1}$$

$$\frac{d\hat{\phi}_{a,b}}{d\hat{x}}=-\xi_{a,b}\frac{d\widehat{T}_{a,b}}{d\hat{x}}-\lambda_{a,b}\widehat{I}_{a,b}, \tag{2}$$

$$\hat{\phi}_b(\hat{x}=1)-\hat{\phi}_a(\hat{x}=1)=\widehat{I}_b. \tag{3}$$

The complete model for a rectangular couple with insulated leg sides and two legs electrically in series, **a** and **b**, is described in terms of dimensionless parameters. The assumed dimensionless variables of the model include a space coordinate $\hat{x}=x/L$ normalized with leg length, temperature $\widehat{T}=T/\Delta T$ normalized with the temperature difference driving the Seebeck effect, voltage $\hat{\phi}=\phi/(\Delta\alpha\cdot\Delta T)$ normalized with a characteristic couple open circuit voltage due to couple Seebeck coefficient $\Delta\alpha=\alpha_b-\alpha_a$ and electrical current $\widehat{I}=IR/(\Delta\alpha\cdot\Delta T)$ normalized with characteristic load resistance R and open circuit voltage. Substitution of the dimensionless parameters into the governing equation results in a set of characteristic parameters which govern the behavior of all couples and provide validation for assumptions. The effect of Thomson heat is captured in the dimensionless parameter $\beta=\tau\Delta\alpha\Delta TL/(ARk)$, which serves as a measure of the accuracy of neglecting Thomson heat τ, in terms of couple Seebeck $\Delta\alpha$, operating temperature difference ΔT, length L, cross sectional area A, load resistance R, and thermal conductivity k. This heat is classically neglected as part of the assumption of constant material properties by the second Kelvin relation $\tau=T\frac{d\alpha}{dT}$ [1,2]. Work in accounting for this heat has been performed by Sherman et al. [10], Yamashita [11], and Min et al. [12]. For β values much smaller than unity the assumption of neglecting Thompson heat is valid, but in the case of a couple with β on the order of unity this assumption is no longer justified. Notice the term involves not only material properties but also a geometric slenderness ratio L/A as well as operational parameters ΔT and R. The effect of Joule heating is captured by the dimensionless parameter $\gamma=\Delta\alpha^2\Delta TL^2/(A^2R^2k\sigma)$, with the introduction of electrical conductivity σ. The dimensionless voltage due to Seebeck effect is captured by $\xi=\alpha/\Delta\alpha$, and the voltage due to electrical losses is found in $\lambda=L/(AR\sigma)$.

Included in the model are the eight boundary conditions required for complete specification of the problem statement. Under a strict set of simplifying assumptions the model can be seen to return the same solution classically offered as the analytic solution of a thermoelectric couple, see Sherman et al. [10], Lampinen [13], or Bejan [14]. These assumptions include: constant isotropic material properties, fixed hot and cold shoe temperatures, insulated leg sides, steady state, and one dimensional conduction. Additionally, due to the electrical series nature of the couple the electrical current in legs **a** and **b** are equal in magnitude and opposite in direction. With appropriate application of aforementioned boundary conditions and solution of the coupled equations the classic solution of the couple can be found.

Calculation of the couple's thermodynamic conversion efficiency reveals two critical design parameters, well suited for optimization of device design: (i) the geometric factor $X=A_bL_a/(A_aL_b)$ is the ratio of the leg slenderness for **a** and **b** legs and (ii) the load factor $Y=R/(L_a/(A_a\sigma_a)+L_b/(A_b\sigma_b))$ is a ratio of load resistance to couple resistance. Details of the classic optimization can be found in literature and provide a means of calculating the optimized X and Y values to obtain a couple with maximum conversion efficiency [10,13–15]. In addition to the device design optimization, the traditional thermoelectric figure of merit can be extracted from this conversion efficiency and used as a material design guideline.

Similarly the method can be applied to a cylindrical couple configured with radial heat transfer. *Legs in a cylindrical couple are configured as a solid washer or ring shape with the temperature gradient ranging from the inside to outside radius*. Sets of p- and n-type washers can be electrically connected in series to complete a circuit (Fig. 1), similar to their rectangular counterparts. Cylindrical couples may prove to be well suited for the design of compact heat exchangers which require a radial conduction path. For instance, the cylindrical couple would serve well in an energy harvesting application of a coolant line passing through a hot exhaust chamber. The outside radius of the legs would be in communication with the hot ambient thermal reservoir, and the cold junction would be in direct thermal contact with a coolant fluid. Cylindrical couples have been theoretically and experimentally investigated by Min and Rowe [16,17], Landecker [18], Lund [19], and Liu [20]. The previous governing equations Eqs. (1)–(3) can be substituted for their cylindrical equivalents and solved, see Appendix A. The temperature and voltage profiles, now functions of radius r and leg width w, can be used to calculate the couple's thermodynamic conversion efficiency. Again, two design parameters, with similar physical meaning to their rectangular counterparts, can be extracted. The appropriate geometric factor as derived by this work becomes $X=w_b\ln\frac{r_{o,a}}{r_i}\Big/\Big(w_a\ln\frac{r_{o,b}}{r_i}\Big)$ with subscript **o** indicating outside radius and **i** inside radius. Likewise the new cylindrical load factor derived in this work becomes $Y=R\Big/\Big(\ln\frac{r_{o,a}}{r_i}/(2\pi\sigma_aw_a)+\ln\frac{r_{o,b}}{r_i}/(2\pi\sigma_bw_b)\Big)$. Optimization of the efficiency in terms of the cylindrical X and Y design factors is identical to the rectangular case and results in the same final optimized values, as suggested by Min and Rowe [16]. The similarity of the rectangular and cylindrical solutions is expected and reported in literature,

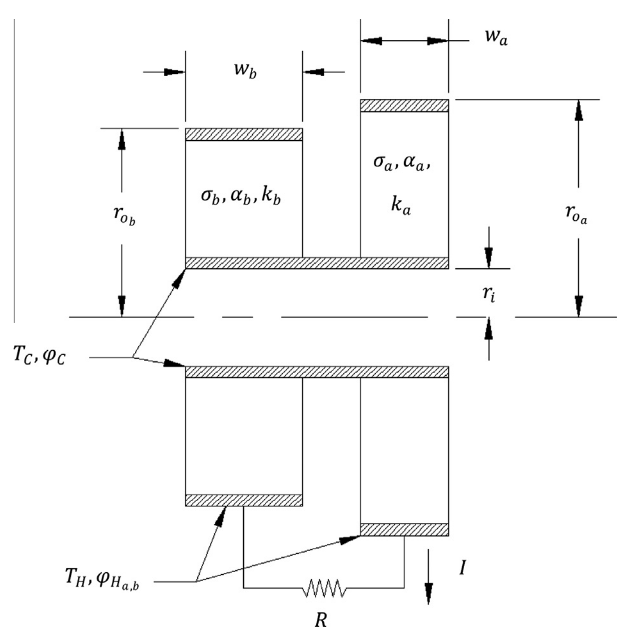

Fig. 1. Schematic of a cylindrical couple, highlighting the geometric parameters of interest leg width w, and inner and outer radius r_i and r_o.

but the new cylindrical X and Y design factors of this work are required to optimize a cylindrical couple. For instance, the new geometric factor and load factor allow one to realize the maximum theoretical conversion efficiency or power density in terms of couple radius and leg width. The classic rectangular design factors do not capture geometries useful to a cylindrical couple.

A useful presentation of the classic solution, Fig. 2, displays the behavior of the couple across the design space. *The contour presentation allows for a better physical understanding of design tolerance factors over the simple analytic solution*. The axes of the plot map out a range of X and Y design factors and the contour lines mark the various levels of calculated conversion efficiency η. *In addition to conversion efficiency, lines of constant power density, electrical current, or power may also be superimposed to assist in couple design*. The location of the maximum coincides with the classic analytic solution, and the figure provides a view into the range of design values which will return nearly optimized couples. Two modifications were introduced to this classical solution with the new design space to optimize the device design for more realistic conditions. These modifications include: (i) variable boundary conditions and (ii) lateral heat transfer.

Throughout this work the material properties employed for the models were selected to represent NASA's general purpose heat source radioisotope thermoelectric generator (GPHS-RTG). The Si/Ge couples have an average n-leg thermal conductivity of 4.02 W/(mK), electrical conductivity of 5.44e4 S/m, and Seebeck coefficient of −231 μV/K. The p-leg has an average thermal conductivity of 4.24 W/(mK), electrical conductivity of 4.33e4 S/m, and Seebeck coefficient of +208 μV/K [21].

2. Variable boundary conditions

In real life applications the temperatures of the hot and cold reservoirs are known; the difference of which can be much different than the temperature drop across the legs due to factors such as conductive resistance of the shoes t/k, interface resistances $h_{interface}$, and convection $h_{h,c}$ or radiation resistance between thermal reservoirs and the shoes. Therefore in device design it is important to leave the thermal boundary conditions of the legs free. This can be achieved by introduction of an effective convection coefficient.

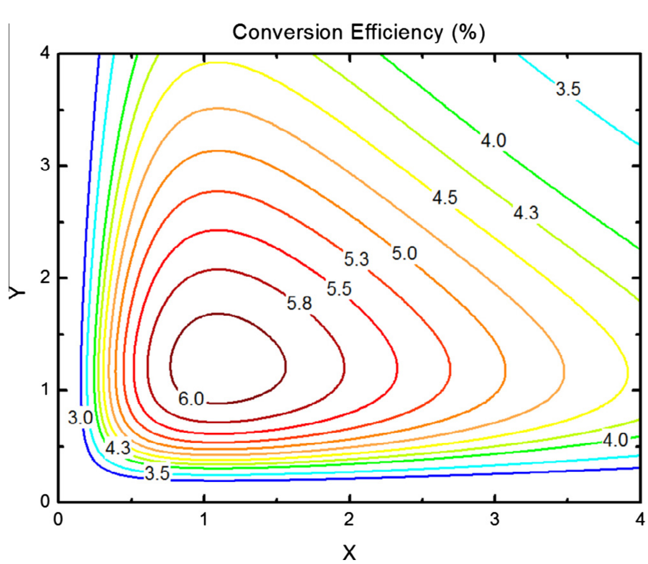

Fig. 2. Contour plot of conversion efficiency for silicon germanium couple, using the classic assumptions.

$$\hbar_{h,c}^{-1} = h_{h,c}^{-1} + h_{interface}^{-1} + \sum_i \frac{t_i}{k_i}. \tag{4}$$

This effective convection coefficient boundary condition can be used to represent an equivalent thermal resistance of a lumped combination of the aforementioned factors. The appropriate thermal boundary conditions to apply to the model are

$$-k_{a,b}\frac{dT_{a,b}(0)}{dx} + \frac{I_{a,b}\alpha_{a,b}}{A_{a,b}}T_{a,b}(0) = \hbar_h\left[T_{\infty_h} - T_{a,b}(0)\right], \tag{5}$$

$$-k_{a,b}\frac{dT_{a,b}(L_{a,b})}{dx} + \frac{I_{a,b}\alpha_{a,b}}{A_{a,b}}T_{a,b}(L_{a,b}) = \hbar_c\left[T_{a,b}(L_{a,b}) - T_{\infty_c}\right], \tag{6}$$

where $\hbar_h$ and $\hbar_c$ are the effective convection coefficients of the hot ($x = 0$) and cold ($x = L$) shoes respectively and $T_{\infty_{h,c}}$ are the ambient reservoir temperatures. The dimensional forms of the boundary conditions are presented for convenience. The first term which accounts for the conductive heat, and the last term which accounts for convective heat are the classic boundary condition used for a non-thermoelectic conductor, see Arpaci [3]. The Peltier heat is introduced by the second term on the left hand side of the boundary condition. Constant material properties and a negligible Thomson heat term are used with the model. As discussed previously the Thomson heat term is negligible for constant material properties through the second Kelvin relation [1]. Solution using the full boundary condition proceeds with a straightforward uncoupling of the differential equations, resulting in a nonlinear expression to solve for the electrical current. The solution with the actual boundary conditions as described is solvable but makes obtaining a closed form efficiency equation difficult; optimization can still be performed numerically and will stand to justify the simplifying assumption of neglecting the Peltier heat term from the boundary. The simplified boundary condition leads to a useful solution of the couple, which allows shoe temperature the freedom to float with the solution as desired. The solution introduces a Device Design Factor, a dimensionless parameter of range zero to one, with the ideal device having a value of unity.

$$\text{Device Design Factor}: \ D_{a,b} = \frac{1}{1 + \frac{k_{a,b}(\hbar_h + \hbar_c)}{L_{a,b}\hbar_h\hbar_c}}. \tag{7}$$

In the limit of effective convection coefficients approaching infinity this Device Design Factor approaches unity and the entire model reduces to the classic solution with the ambient temperatures replacing the shoe operating temperatures. *For a real couple the Design Factor serves as an approximation of the operating temperature in terms of the ambient temperature*. The couple's realized temperature difference can be estimated by an effective temperature, $\Delta T_{Effective} = (D_a + D_b)\Delta T_\infty/2$, an estimation of the actual temperature difference in terms of the Design Factor and ambient temperatures. This effective temperature can be used both to assist in couple design as well as thermoelectric module integration in a system. The Device Design Factor plays a significant but indirect role in the couple's Thomson heat and Joule heating terms (Eq. (1)) by altering the operating temperatures of the couple and thereby altering the couple's operating electrical current. The Fourier heat term of the couple is also influenced by the Device Design Factor as thermal gradients are fixed by the couple's operating temperatures.

Thermodynamic conversion efficiency η for the convection boundary condition can be derived in terms of the Design Factor D with the simplifying assumption of $\hbar_h = \hbar_c$ and by assuming that the hot shoe temperature can be approximated with the aforementioned effective couple temperature (ΔT_{Eff}). The $\hbar_h = \hbar_c$ assumption is only required to obtain clean and meaningful solutions for

presentation; this assumption is not required to hold for the general application of the model.

$$\eta = \frac{\eta_{c_\infty} Y}{\frac{(1+Y)^2}{T_{\infty_h} Z_D(X, D_a, D_b)} + \frac{(1+Y)(\alpha_b - \alpha_a)}{D_b\alpha_b - D_a\alpha_a}\left[1 - \frac{\eta_{c_\infty}}{2}\left(1 - \frac{D_a + D_b}{2}\right)\right] - \frac{\eta_{c_\infty}}{2}}, \tag{8}$$

$$Z_D(X, D_a, D_b) = \frac{(D_b\alpha_b - D_a\alpha_a)^2}{\left(\frac{1}{\sigma_a} + \frac{1}{\sigma_b X}\right)(D_a k_a + D_b k_b)}, \tag{9}$$

where Z_D is analogous to the classic dimensionless couple parameter Z used in figure of merit ZT and η_{c_∞} is the thermodynamic Carnot efficiency based on the ambient temperatures. The efficiency can be optimized in terms of the four design parameters X, Y, and $D_{a,b}$ (see Appendix B).

The efficiency increases with increasing D. The optimal value for D is unity – in the range zero to unity – which causes the conversion efficiency to reduce to the conversion efficiency of the classic case, Eq. (8). For a D of unity no losses exist through the shoes and the temperature drop between the hot and cold reservoirs are the same as the temperature drop across the legs.

As a guideline, the efficiency optimized couple should be designed with optimal X and Y values in addition to using long legs, having a high boundary convection coefficient, and as small a leg thermal conductivity as possible. To exemplify this, the dependence of Device Design Factor is illustrated in Fig. 3 as a function of leg length, for a wide range of convection coefficients. For the clarity of this demonstration only shoe conduction resistance was taken into account, neglecting additional terms such as the interface resistance and shoe convection. A shoe convection coefficient can be approximated as the thermal conductivity of shoe material divided by the shoe thickness using Eq. (4); for instance a 1.9 mm thick SiMo shoe would have roughly 13,000 W/(m^2 K). The typical shoe used in the GPHS-RTG is 1.9 mm thick SiMo [21,22]. *The practical design rule stands to design a short couple, in order to produce the largest power, without reducing the Design Factor significantly*. For example, for legs shorter than 10 mm and a shoe convection coefficient of 50,000 W/(m^2 K), the Design Factor starts diverging from unity (Fig. 3). In the case of 1.9 mm thick SiMo shoe, with the conduction resistance of 13,000 W/(m^2 K), legs shorter than 10 mm will start exhibiting non-trivial divergence from unity, typical GPHS-RTG legs are sufficiently designed to be 20.3 mm [22]. Furthermore, this divergence will occur at longer leg lengths as the (i) shoe thickness increases, (ii) the conductivity of the shoe material decreases, and (iii) other factors such as convection and interface resistance are included. In an application such as NASA's GPHS-RTG where the heat source is in direct contact with the shoe, the conduction resistance will dominate, however in other possible industrial applications (i.e., exhaust of automobiles) the convection will become the dominant factor with practical convection coefficients in the range of 5–50 W/(m^2 K) [23]. In such applications, the importance of this design parameter becomes even more significant due to large divergence from unity. *While the classic solution predicts the same conversion efficiency of a couple of any length this model analytically demonstrates the effect of length with the introduction of Design Factor*. A couple with Design Factor near unity approaches the maximum conversion efficiency as predicted by classic theory, while a reduced factor will have significant reductions on efficiency. As a result of the model a couple's length can be devised in order to bring the Design Factor satisfactorily close to unity, a reasonable value for Design Factor may be selected to have a value such as 0.99 so we can then calculate the length required to reach this level as $L_{99\%}$.

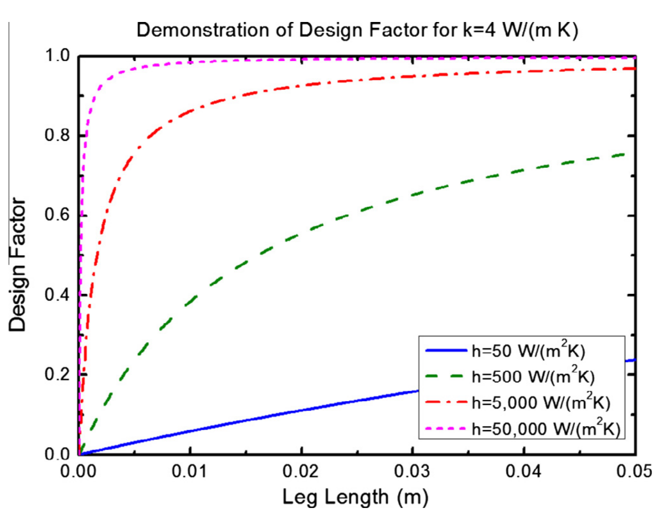

Fig. 3. Device Design Factor as a function of leg length for a range of convection coefficients.

$$L_D = \frac{D(\hbar_h + \hbar_c)k}{(1-D)\hbar_h\hbar_c} \quad \text{for instance } L_{99\%} = \frac{99k(\hbar_h + \hbar_c)}{\hbar_h\hbar_c}. \tag{10}$$

Eqs. (8)–(10) provide a complete description of the thermoelectric conversion efficiency of a couple, taking into account total thermal resistance of shoes. The solution is consistent with the classic case of fixed hot and cold temperatures in which convection coefficients can be thought of as being infinite resulting in Design Factors of unity.

To this point the formulation has neglected the Peltier term in the boundary condition, in order to obtain the desired analytic efficiency equation (Eq. (8)). A solution including the Peltier term has been optimized numerically and provides a contrast for the simplified analytic model. A comparison of the approximate boundary condition with the exact boundary condition is presented in Table 1. The table displays the X_{opt} and Y_{opt} values required to obtain the optimal conversion efficiency η_{opt}. The X_{opt}, Y_{opt}, and η_{opt} values are calculated for both the analytic and the exact solutions over a range of boundary convection coefficients. For an infinite convection coefficient, Design Factor 1.0, the analytic solution is identically equal to the exact solution. For large coefficients, greater than 50,000 W/(m^2 K), the difference between the analytic model and the exact solution are negligible. For convection coefficients below 5000 W/(m^2 K), Design Factor 0.85, the difference between the analytic model and the exact solution becomes apparent. At a convection coefficient of 5000 W/(m^2 K) the difference in the analytically calculated conversion efficiency (5.30%) and the exact solution (5.26%) contains less than a 1% difference. Similarly the differences between the analytic and exact models are less than 1% for the X_{opt} and Y_{opt} values. Lower convection coefficients lead to larger differences between the analytic model and the exact solution. For a convection coefficient of 500 W/(m^2 K), Design factor 0.37, the difference between the analytic conversion efficiency (2.37%) and the exact solution (2.28%) is 3.9%. The analytic model, using the simplified boundary condition, is found to be reasonably close to the exact solutions. The simplification is valid in the case $\alpha\Delta\alpha\Delta TL/(ARk) \ll 1$.

3. Lateral heat transfer

The primary heat transfer in a thermoelectric couple is down the leg length, although some heat will travel in the lateral direction into the region between legs or from the region between legs into the couple. Insulating the volume between the legs, or operating in a vacuum will reduce this effect. However, it is of interest to investigate the magnitude of such lateral heat transfer on the

Table 1
Comparison of simplified boundary condition to numerical solution of actual condition.

B.C. convection [W/(m^2 K)]	Design Factor [–]	X_{opt} (Eq. (B.8)) [–]	Y_{opt} (Eq. (B.9)) [–]	η_{opt} (Eq. (8)) [%]	X_{opt} exact [–]	Y_{opt} exact [–]	η_{opt} exact [–]
∞	1.00	1.09	1.22	6.15	1.09	1.22	6.15
500,000	0.99	1.09	1.22	6.14	1.09	1.22	6.14
50,000	0.98	1.09	1.22	6.05	1.09	1.22	6.05
5000	0.85	1.10	1.22	5.30	1.09	1.23	5.26
500	0.37	1.11	1.22	2.37	1.09	1.27	2.28

thermoelectric couple's operation in order to determine critical design considerations.

The lateral heat transfer can be considered using a one dimensional thermoelectric conduction equation, derived for a control volume which extends across the width of a leg so as to include heat transfer at the boundary as part of the governing equation. In this fashion the formulation resembles the classic heat transfer in a fin [3–5]. The modified thermal governing equations now include a Fin Factor, a dimensionless parameter with the ideal device having a value of zero.

$$\text{Fin Factor}: \quad F = L\sqrt{\frac{Ph}{kA}}, \tag{11}$$

where the leg perimeter P, and side convection coefficient h have now been introduced. Similar to the convection boundary condition solution, the leg side convection coefficient may be an effective coefficient to account for any mode of heat transfer. The Fin Factor is found only in an additional lateral heat transfer term, which must be included in the thermal governing equation. The Fin Factor plays no role in altering the Fourier, Thomson, or Joule heating terms. The thermal governing equations now become

$$-\frac{d^2\hat{\theta}_{a,b}}{d\hat{x}^2} + \beta_{a,b}\hat{I}_{a,b}\frac{d\hat{\theta}_{a,b}}{d\hat{x}} + F^2_{a,b}\hat{\theta}_{a,b} - \gamma_{a,b}\hat{I}^2_{a,b} = 0. \tag{12}$$

A change of variables has been performed as $\theta(x) = T(x) - T_\infty$ with T_∞ the ambient leg side temperature, assumed to be fixed along the leg length for simplicity. In fact the ambient temperature, which the leg communicates with, may be a function of space, but the fixed ambient temperature approximation allows for insightful investigation without unneeded complexity. The dimensionless temperature is now defined as $\hat{\theta}(x) = \theta(x)/\Delta T$. The remainder of the model consists of Eqs. (2) and (3) in their presented form as the leg sides are still assumed to be electrically insulated. Following the previous case the Thomson heat term will be neglected and constant material properties will be assumed. Solution of the temperature profile is found to be hyperbolic in the space coordinate, in accordance with a fin type formulation. The electrical current reduces to the same result as the classic case, as expected.

The inclusion of an ambient temperature introduces an inflection point, near the ambient temperature, into the thermal solution, shown exaggerated in Fig. 4 by employing a large convection coefficient $h = 500\ \text{W}/(\text{m}^2\ \text{K})$. A practical convection coefficient may be in the range of 5–50 W/(m^2 K) [23]. The electrical current is fixed to that calculated in the classic solution; therefore the power output of the fin couple is limited to the classic solution, thus for a system that is constructed to have Design Factor of unity. *Any couple which produces the same power output but draws a larger heat input or rejects a larger heat output will be a less efficient device.*

The four cases in Fig. 4 have hot and cold end temperatures of 1123 and 573 K, respectively. The profiles are generated with $X = 1$ and $Y = 1$ for convenience, as these are typical values used in practice. Since the electrical solution is the same in all four cases both the power output and the Peltier heat terms are identical.

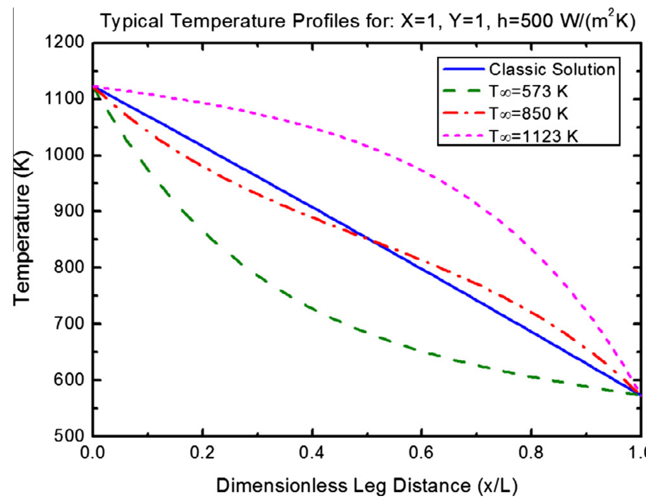

Fig. 4. Typical temperature profiles for a range of ambient temperatures, with $X = 1$ and $Y = 1$ for convenience.

Therefore the difference in conversion efficiency is determined from the lateral heat transfer and the conductive heat transfer through the ends of the legs. The heat transferred through the ends of the legs is proportional to the temperature gradient at the ends. For the extreme case of an ambient temperature equal to that of the cold shoe, lateral heat can transfer only out of the device and a larger heat input is drawn for the same power output; thus the couple will be less efficient then the classic case. From Fig. 4 this case can be seen to have a steeper temperature gradient at the hot shoe, compared to the classic solution, confirming the larger heat input. In the other extreme, the case of ambient temperature equal to that of the hot shoe, the couple will again produce the same power output and Peltier heat. In this case lateral heat is transferred only into the couple, so the output thermal energy is directly proportional to the thermal gradient at the cold shoe. Compared to the classic solution this case will have a larger heat output for the same power generation, so the couple will be less efficient. Thus any intermediate temperature can follow similar reasoning to be less efficient then the classic case. However, for intermediate temperatures the lateral heat will pass into the leg along some portion of the length, and out of the leg along the remainder. Therefore, the evaluation of conversion efficiency becomes more involved; see Appendix C for an example. Fig. 4 shows exaggerated profiles by employing a large convection coefficient.

The efficiency equation is given below for the case of ambient temperature equal to the cold shoe temperature. Two new geometric factors, a thermal fin geometric factor (G), and an electrical fin geometric factor (H) are defined. In the limit of Fin Factor (F) approaching zero – the ideal couple – both G and H approach the traditional geometric factor X. Although only F_a is found in the efficiency equation, the influence of both leg's fin factors (F_a and F_b) impact the efficiency through the introduction of the geometric factors G and H.

$$\eta = \frac{\eta_c Y}{\frac{F_a(1+Y)^2}{\tanh(F_a) T_h Z_F(X,G)} + (1+Y) - \eta_c \frac{\tanh\left(\frac{F_a}{2}\right)\left(\frac{1}{\sigma_a}+\frac{1}{H\sigma_b}\right)}{F_a\left(\frac{1}{\sigma_a}+\frac{1}{X\sigma_b}\right)}}, \tag{13}$$

$$Z_F(X,G) = \frac{(\alpha_b - \alpha_a)^2}{\left(\frac{1}{\sigma_a}+\frac{1}{X\sigma_b}\right)(k_a + Gk_b)}, \tag{14}$$

$$G(F) = \sqrt{\frac{P_b A_b h_b k_a}{P_a A_a h_a k_b}} \frac{\tanh(F_a)}{\tanh(F_b)}, \tag{15}$$

$$H(F) = \sqrt{\frac{P_b A_b h_b k_a}{P_a A_a h_a k_b}} \frac{\tanh(\frac{F_a}{2})}{\tanh(\frac{F_b}{2})}, \tag{16}$$

where Z_F is analogous to the classic dimensionless couple parameter Z used in figure of merit ZT and η_c is the thermodynamic Carnot efficiency. The conversion efficiency of the fin couple simplifies to the classic solution when F approaches zero as $F/\tanh(F)$ approaches unity and $\tanh(F/2)/F$ approaches $1/2$. The design rule stands to design a couple with a P/A ratio small enough to force the Fin Factor satisfactorily near zero. This small P/A ratio requires the use of large cross-sectional area legs; for instance a square cross-section leg will have the P/A ratio inversely proportional to the side length. Therefore, to obtain a small P/A ratio the use of a large side length is required. Using values typical for the NASA GPHS-RTG (legs of $2.74 \times 6.50 \times 20.3$ mm) [22] the Fin Factor as developed in this work could be as large as 0.84 under a He atmosphere testing condition assuming an h of 5 W/(m^2 K). The He atmosphere testing condition is common for pre-mission tests before venting to the vacuum of space [22]. For non-space applications of thermoelectrics, where a vacuum is not available, lateral losses will always be present. *While the classic solution predicts the same conversion efficiency of a couple of any P/A ratio this model analytically demonstrates the effect of P/A with the introduction of Fin Factor*. Similar to the couple length selection of the previous section, to keep Device Design Factor near unity, a P/A ratio can be selected to keep the Fin Factor near zero. A suitably small Fin Factor may be 0.05 so we can then calculate the P/A ratio required to reach this level as $(P/A)_{5\%}$.

$$\left(\frac{P}{A}\right)_F = \frac{F^2 k}{L^2 h} \quad \text{for instance} \quad \left(\frac{P}{A}\right)_{5\%} = \frac{0.05^2 k}{L_{99\%}^2 h}. \tag{17}$$

4. Comparison of models

Table 2 summarizes a set of couple parameters and illustrates how it can reduce conversion efficiency, a hazard of a poorly designed couple. The table is calculated from typical values for couples found in the GPHS-RTG, all cases use matching couple material properties and leg sizes. The parameters of study in the table are the end and side convection coefficients, the calculated Device Design Factor and Fin Factor are also shown. The effect of a range of Design and Fin Factors can be clearly observed on maximum conversion efficiency and power density. The ideal couple, case 1 with Design Factor of unity and Fin Factor of zero, gives the greatest maximum conversion efficiency and power density. In the cases of Design Factor deviating from unity, cases 2–5, significant reductions in both maximum conversion efficiency and power density can be observed. Fin Factor is kept zero for the study of cases 2–5. Case 2 represents a case with very low leg end thermal resistance, such as direct conduction contact, while case 5 represents a condition with significant leg end thermal resistance, typical of a convection coupled device, combined with insufficiently short leg length. Between cases 2 and 5 the conversion efficiency drops from 6.14% to 2.28% and power density drops from 17,670 to 2300 W/m^2. Additionally, the optimal geometric factor X remains unchanged, while the optimal load factor Y shifts with decreasing Design Factor. The reduction in conversion efficiency in case 5 is the result of using the same couple length for an application where it may not be appropriate, as indicated by the low Device Design Factor.

The remaining cases 6–9 show reduced maximum conversion efficiency as a function of an increasing Fin Factor. Device Design Factor is kept to a value of one for cases 6–9. As a result the maximum power density remains constant. The cases 6–9 show the behavior of the leg side convection coefficient, with four orders of magnitude, a range which covers the full span of realistic devices. Between case 6 and 9 convection coefficient varies from 0.5 to 500 W/(m^2 K) with a resulting change in conversion efficiency from 6.14% to 2.70%. The location of both the optimal X and Y parameters shift as a function of the Fin Factor.

The reductions in conversion efficiency and power density suggest a strong need to consider additional design parameters than simply the material figure of merit. The design factors introduced, along with Eqs. (8) and (13), provide a simple means of evaluating couple design without requiring lengthy work with numerical simulations. Additionally, the parameters of study introduced in this work serve to help map out efficient testing matrices for experimental work. For instance the Device Design Factor and Fin Factor incorporates the influence of several couple properties and can save the experimentalist the time of studying the influence of each property individually.

Table 2 may serve as both a guide for model verification and to assist in device design. The change in conversion efficiency and power density as a function of Device Design Factor may be verified experimentally by creating a set of couples with the appropriate Design Factors as outlined by cases 2–5. This could be accomplished by either fixing the leg properties while varying the thermal resistance of the shoes (i.e. altering the shoe thickness or material), or alternatively by allowing the leg length to vary for

Table 2
Comparison of couple parameters demonstrating the importance of considering several factors.

Case #	B.C. convection [W/(m^2 K)]	Leg side convection [W/(m^2 K)]	Design Factor [–]	Fin Factor [–]	Max efficiency [%]	Efficiency optimized		Max power density [W/(m^2)]
						X_{opt}	Y_{opt}	
1	∞	0	1.00	0.00	6.15	1.09	1.22	17,733
2	500,000	0	0.99	0.00	6.14	1.09	1.22	17,670
3	50,000	0	0.98	0.00	6.05	1.09	1.22	17,118
4	5000	0	0.86	0.00	5.26	1.09	1.23	12,780
5	500	0	0.38	0.00	2.28	1.09	1.27	2300
6	∞	0.5	1.00	0.09	6.14	1.09	1.22	17,733
7	∞	5	1.00	0.32	6.05	1.10	1.21	17,733
8	∞	50	1.00	1.00	5.33	1.20	1.19	17,733
9	∞	500	1.00	3.16	2.70	1.59	1.09	17,733

fixed shoe resistance. Through this study it should be verified that Eq. (10) provides the minimum leg length to reduce influence of the shoe thermal resistance; thereby providing the device designer with a single simple guideline for leg length. Similarly cases 6–9 can be experimentally verified by creating a set of couples with varying cross-sectional area. A set of couples could be created with varying leg side thickness, selected in such a way as to generate a range of perimeter to area ratios which can satisfy the Fin Factors outlined in the table. The influence of Fin Factor on conversion efficiency and the independence of Fin Factor on power should be verified. Additionally, Eq. (17) should be verified to provide the required perimeter to cross-sectional area ratio. The proper ratio is needed to reduce the influence of lateral heat transfer.

5. Conclusion

The influence of thermal resistance and lateral heat transfer on the behavior of a thermoelectric couple has been investigated analytically. The analytic approach, as opposed to numerical simulations, offers convenient closed form efficiency equations in terms of the introduced parameters Device Design Factor and Fin Factor. Using realistic values of the Device Design Factor such as 0.38 a reduction in maximum conversion efficiency from 6.15% to 2.28% is calculated. This factor accounts for the thermal resistance inherent to any actual thermoelectric device. Using practical values of the Fin Factor such as 1.00 a reduction in maximum conversion efficiency from 6.15% to 5.33% is calculated. This factor accounts for the lateral heat which can transfer through the sides of a thermoelectric leg. Practical and simple design guidelines for the $L_{99\%}$ and $(P/A)_{5\%}$ couple parameters have been generated to assist in couple design, without requiring the need for detailed numerical work. Additionally, the work has been completed for both the common rectangular couples and the practically interesting cylindrical couples, for which the appropriate geometric factor X and electrical factor Y have been derived in terms of cylindrical parameters.

Acknowledgments

The authors gratefully acknowledge the National Aeronautics and Space Administration for their financial support of this work (NASA/USRA contract 04555-004). The authors would also like to thank Benjamin Kowalski for helpful discussion.

Appendix A. Details of the cylindrical solutions

The cylindrical thermal equation used to obtain the cylindrical form of the design parameters X and Y is expressed in terms of radius r rather than the spacial rectangular coordinate x. The dimensional form of the governing equation is

$$\frac{d}{dr}\left(-k_{a,b}r\frac{dT_{a,b}}{dr}\right)+\frac{I_{a,b}\tau_{a,b}}{2\pi w_{a,b}}\frac{dT_{a,b}}{dr}-\frac{I_{a,b}^2}{4\pi^2 w_{a,b}^2 r\sigma_{a,b}}=0. \tag{A.1}$$

The solution of the cylindrical thermal gradient is

$$\frac{dT_{a,b}}{dr}=-\frac{I_{a,b}^2}{4\pi^2 w_{a,b}^2 r\sigma_{a,b}k_{a,b}}\ln r+\frac{I_{a,b}^2}{8\pi^2 w_{a,b}^2 r\sigma_{a,b}k_{a,b}}\left[\frac{(\ln r_i)^2-(\ln r_o)^2}{\ln r_i-\ln r_o}\right]-\frac{\Delta T}{r(\ln r_i-\ln r_o)}. \tag{A.2}$$

The cylindrical electrical current solution is

$$I=\frac{(\alpha_b-\alpha_a)\Delta T}{\frac{\ln r_i/r_{o_b}}{2\pi w_b\sigma_b}+\frac{\ln r_i/r_{o_a}}{2\pi w_a\sigma_a}+R}. \tag{A.3}$$

Appendix B. Details of the variable boundary condition solutions

The variable boundary condition solution, with the simplifying approximation of neglecting Peltier heat term, results in the following thermal gradient profile

$$\frac{dT_{a,b}}{dx}=-\frac{I_{a,b}^2}{A_{a,b}^2\sigma_{a,b}k_{a,b}}x+\frac{I_{a,b}^2L_{a,b}}{2A_{a,b}^2\sigma_{a,b}k_{a,b}}\frac{L_{a,b}\hbar_h\hbar_c}{\omega_{a,b}}\left(1+\frac{2k_{a,b}}{L_{a,b}\hbar_c}\right)-\frac{\hbar_h\hbar_c\Delta T_\infty}{\omega_{a,b}}, \tag{B.1}$$

$$\text{where } \omega_{a,b}=k_{a,b}(\hbar_h+\hbar_c)+L_{a,b}\hbar_h\hbar_c. \tag{B.2}$$

The variable boundary condition electrical current solution is

$$I=\frac{-\delta_2\pm\sqrt{\delta_2^2-4\delta_1\delta_3}}{2\delta_1}, \tag{B.3}$$

$$\text{where } \delta_1=\frac{\alpha_bL_b^2}{2A_b^2\sigma_bk_b}\left[1-\frac{\hbar_h}{\omega_b}(L_b\hbar_c+2k_b)\right]-\frac{\alpha_aL_a^2}{2A_a^2\sigma_ak_a}\left[1-\frac{\hbar_h}{\omega_a}(L_a\hbar_c+2k_a)\right], \tag{B.4}$$

$$\text{where } \delta_2=-\left(\frac{L_b}{A_b\sigma_b}+\frac{L_a}{A_a\sigma_a}+R\right), \tag{B.5}$$

$$\text{where } \delta_3=\left(\frac{\hbar_h\hbar_cL_b}{\omega_b}\alpha_b-\frac{\hbar_h\hbar_cL_a}{\omega_a}\alpha_a\right)\Delta T_\infty. \tag{B.6}$$

For small δ_1 the variable boundary electrical current approaches

$$I\approx\frac{-\delta_3}{\delta_2}=\frac{\left(\frac{\hbar_h\hbar_cL_b}{\omega_b}\alpha_b-\frac{\hbar_h\hbar_cL_a}{\omega_a}\alpha_a\right)\Delta T_\infty}{\frac{L_b}{A_b\sigma_b}+\frac{L_a}{A_a\sigma_a}+R}. \tag{B.7}$$

The conversion efficiency (Eq. (8)) of a variable boundary couple is optimized with the following parameters

$$X_{\eta_{opt}}=\sqrt{\frac{k_a\sigma_aD_a}{k_b\sigma_bD_b}}, \tag{B.8}$$

$$Y_{\eta_{opt}}=\sqrt{1+Z_D(X_{\eta_{opt}},D_a,D_b)\left[T_{\infty_h}\frac{\alpha_b-\alpha_a}{D_b\alpha_b-D_a\alpha_a}\left(1-\frac{D_a+D_b}{2}\right)-\frac{\Delta T_\infty}{2}\right]}, \tag{B.9}$$

$$Z_D(X_{\eta_{opt}},D_a,D_b)=\frac{(D_b\alpha_b-D_a\alpha_a)^2}{\left(\sqrt{\frac{k_aD_a}{\sigma_a}}+\sqrt{\frac{k_bD_b}{\sigma_b}}\right)^2}. \tag{B.10}$$

Appendix C. Details of the lateral heat solutions

The lateral heat transfer solution thermal gradient is

$$\frac{dT_{a,b}}{dx}=m_{a,b}C_{1_{a,b}}\exp(xm_{a,b})+m_{a,b}C_{2_{a,b}}\exp(-xm_{a,b}), \tag{C.1}$$

$$\text{where } m_{a,b}=\sqrt{\frac{P_{a,b}h_{a,b}}{k_{a,b}A_{a,b}}}, \tag{C.2}$$

$$\text{where } C_{1_{a,b}}=\theta_h+\frac{\theta_c-\theta_h\exp(m_{a,b}L_{a,b})}{2\sinh(m_{a,b}L_{a,b})}+\frac{I_{a,b}^2}{P_{a,b}A_{a,b}\hbar_{a,b}m_{a,b}^2\sigma_{a,b}}\left[\frac{\exp(m_{a,b}L_{a,b})-1}{2\sinh(m_{a,b}L_{a,b})}-1\right], \tag{C.3}$$

where $$C_{2_{a,b}} = \frac{\theta_h \exp(m_{a,b}L_{a,b}) - \theta_c}{2\sinh(m_{a,b}L_{a,b})} - \frac{I_{a,b}^2}{P_{a,b}A_{a,b}\hbar_{a,b}m_{a,b}^2\sigma_{a,b}} \times \frac{\exp(m_{a,b}L_{a,b}) - 1}{2\sinh(m_{a,b}L_{a,b})}. \tag{C.4}$$

The electrical current of the lateral heat transfer couple is identical to the classic solution

$$I = \frac{(\alpha_b - \alpha_a)\Delta T}{\frac{L_b}{A_b\sigma_b} + \frac{L_a}{A_a\sigma_a} + R}. \tag{C.5}$$

The conversion efficiency of a lateral heat transfer couple must be calculated in such a fashion as to include the lateral heat. This can be accomplished as follows

$$\eta = \frac{I^2R}{-k_aA_a\frac{dT_a(0)}{dx} - k_bA_b\frac{dT_b(0)}{dx} + I(\alpha_bT_b(0) - \alpha_aT_a(0) + Q_{Lateral}}, \tag{C.6}$$

$$Q_{Lateral} = \int_{\chi_a}^{L_a} h_aP_a(T_\infty - T_a(x))dx + \int_{\chi_b}^{L_b} h_bP_b(T_\infty - T_b(x))dx, \tag{C.7}$$

$$\chi_{a,b} = \ln\left[\frac{-\frac{I_{a,b}^2}{P_{a,b}A_{a,b}\hbar_{a,b}m_{a,b}^2\sigma_{a,b}} \pm \sqrt{\left(\frac{I_{a,b}^2}{P_{a,b}A_{a,b}\hbar_{a,b}m_{a,b}^2\sigma_{a,b}}\right)^2 - 4C_{1_{a,b}}C_{2_{a,b}}}}{2C_{1_{a,b}}}\right]\frac{1}{m_{a,b}}. \tag{C.8}$$

References

[1] Onsager Lars. Reciprocal relations in irreversible processes II. Phys Rev 1931;38:2265–79.
[2] Onsager Lars. Reciprocal relations in irreversible processes I. Phys Rev 1931;37:405–26.
[3] Arpaci, Conduction heat transfer. Addison-Wesley Pub. Co.; 1966.
[4] Ozisik, Heat transfer: a basic approach. McGraw-Hill; 1985.
[5] Carslaw H, Jaeger J. Conduction of heat in solids. Clarendon Press; 1986.
[6] Meng Jing-Hui, Wang Xiao-Dong, Zhang Xin-Xin. Transient modeling and dynamic characteristics of thermoelectric cooler. Appl Energy 2013;108:340–8.
[7] Alata M, Al-Nimr MA, Naji M. Transient behavior of a thermoelectric device under the hyperbolic heat conduction model. Int J Thermophys 2003;24(6):1753–68.
[8] Montecucco A, Buckle JR, Knox AR. Solution to the 1-D unsteady heat conduction equation with internal Joule heat generation for thermoelectric devices. Appl Therm Eng 2012;35:177–84.
[9] Sandoz-Rosado Emil, Stevens Robert. Robust finite element model for the design of thermoelectric modules. J Electron Mater 2010;39(9):1848–55.
[10] Sherman B, Heikes RR, Ure RW. Calculation of efficiency of thermoelectric devices. J Appl Phys 1960;31(1):1.
[11] Yamashita Osamu. Effect of linear and non-linear components in the temperature dependences of thermoelectric properties on the cooling performance. Appl Energy 2009;86(9):1746–56.
[12] Min Gao, Rowe DM, Kontostavlakis K. Thermoelectric figure-of-merit under large temperature differences. J Phys D: Appl Phys 2004;37(8):1301–4.
[13] Lampinen MJ. Thermodynamic analysis of thermoelectric generator. J Appl Phys 1991;69:4318.
[14] Bejan A. Advanced engineering thermodynamics. Wiley; 2006.
[15] Goldsmid HJ. CRC handbook of thermoelectrics. In: Rowe DM, editor. CRC handbook of thermoelectrics. CRC Press; 1995. p. 19–25.
[16] Min G, Rowe DM. Thermoelectric handbook: macro to nano. In: Rowe DM, editor. Thermoelectric handbook: macro to nano. CRC Press; 2006. p. 11.
[17] Min Gao, Rowe DM. Ring-structured thermoelectric module. Semicond Sci Technol 2007;22(8):880–3.
[18] Landecker K. Some aspects of the performance of refrigerating thermojunctions with radial flow of current. J Appl Phys 1976;47:1846.
[19] Lund T. Refrigerating thermojunctions with radial flow of current. J Appl Phys 1978;49(9):4942.
[20] Liu L. A continuum theory of thermoelectric bodies and effective properties of thermoelectric composites. Int J Eng Sci 2012;55:35.
[21] RCA. Silicon germanium thermoelectric materials and module development program (U). Technical report. RCA topical report; 1969.
[22] Bennett Gary L, Lombardo James J, Hemler Richard J, Silverman Gil, Whitmore CW, Amos Wayne R, et al. The general-purpose heat source radioisotope thermoelectric generator: a truly general-purpose space RTG. In: AIP conference proceedings, vol. 969; 2008. p. 663–71.
[23] Incropera FP, Dewitt D, Bergman T, Lavine A. Introduction to heat transfer. 6th ed. Wiley; 2011.